Parametric scans of HB and LS-RPA regimes employing Petawatt laser

S. Kar[1], K.F. Kakolee[1], B. Qiao[2], D. Doria[1], B. Ramakrishna[1], G. Sarri[1], K. Quinn[1], M. Zepf[1], X. Yuan[3], P. McKenna[3], M. Cerchez[4], J. Osterlholz[4], O. Willi[4], A. Macchi[5], M. Borghesi[1]

[1] *Centre for Plasma Physics, Queen's University Belfast, BT7 1NN, Belfast, UK*

[2] *Center for Energy Research,University of California San Diego, CA 92093-0417 USA*

[3] *Department of Physics, University of Strathclyde, Glasgow, UK*

[4] *Institut für Laser-und Plasmaphysik, Heinrich-Heine-Universit¨at, D¨usseldorf, Germany*

[5] *Dipartimento di Energetica, Università di Roma 1 'La Sapienza', Roma, Italy*

Abstract:

By contrast to the Target Normal Sheath acceleration (TNSA) mechanism [1], Radiation Pressure Acceleration (RPA) is currently attracting a substantial amount of experimental [2,3] and theoretical [4-6] attention worldwide due to its superior scaling in terms of ion energy and laser-ion conversion efficiency. Employing Vulcan Petawatt lasers of the Rutherford Appleton Laboratory, UK, both the Hole-boring (HB) and the Light-Sail (LS) regimes of the RPA have been extensively explored. When the target thickness is of the order of hole-boring velocity times the laser pulse duration, highly collimated plasma jets of near solid density are ejected from the foil, lasting up to ns after the laser interaction. By changing the linear polarisation of the laser to circular, improved homogeneity in the jet's spatial density profile is achieved which suggests more uniform and sustained radiation pressure drive on target ions. By decreasing the target areal density or increasing irradiance on the target, the LS regime of the RPA is accessed where relatively high flux (~ 10^{12} particles/MeV/Sr) of ions are accelerated to ~ 10 MeV/nucleon energies in a narrow energy bandwidth. The ion energy scaling obtained from the parametric scans agrees well with theoretical estimation based on RPA mechanism and the narrow bandwidth feature in the ion spectra is studied by 2D particle-in-simulations.

Experimental Setup:

The experiment was carried out using the VULCAN Nd:glass laser of the Rutherford Appleton Laboratory, U.K., operating in chirped pulse amplification (CPA) mode. The laser wavelength and full width at half maximum (FWHM) pulse duration are 1.053 μm and 750 fs respectively. The laser was focused down on the target at near normal incidence by using an *f*/3 off-axis parabola. In order to reduce the pre-pulses and to suppress the intensity of amplified spontaneous emission, a plasma mirror was employed before the target. A

schematic of the experimental setup is shown in the Fig. 1. A zero order quarter wave plate was used in the focusing beam, before the plasma mirror, in order to change the polarisation of the laser on the target. The intensity on the target was varied from 5×10^{19} W/cm^2 to 3×10^{20} W/cm^2 by increasing the laser spot size on the target, by translating the parabola along the focussing axis. Targets of various materials (Cu, Al, Au and CH) and thickness (10 μm down to 100 nm thickness) were used.

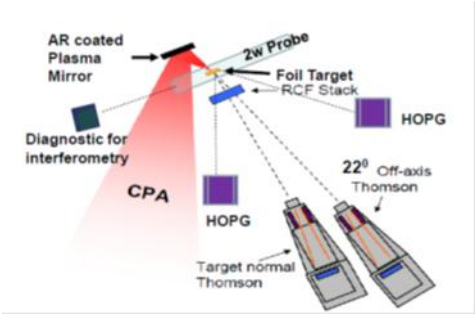

Fig 1. Schematic of the experimental set up.

Two high resolutions Thompson Parabola Spectrometers were fielded in order to measure the ion spectra along the target normal direction and 22^0 off to the target normal. Hydrodynamic expansion of the plasma jets emerged from the target rear surface was characterised by employing transverse Nomarsky interferometer and shadowgraphy with high spatial (few microns) and temporal (ps) resolutions. The setup was designed to achieve two ps snapshots of the interaction at different times in a single shot.

Result and Discussions:

Main results obtained from the experimental campaign, by systematically varying target (material and thickness) and laser (intensity and polarisation) parameters, are discussed below.

(a) Sub-Mev ion jet by HB mechanism

The temporal evolution of the collimated plasma jets at the target rear side was observed from 150 ps to 1.1 ns, after the arrival of the CPA on the target. By comparing the jet expansion velocity at late times, obtained from the analysis of interferograms, with hydrodynamic simulations, an estimation for velocity of ions attained by the HB mechanism is obtained. Fig. 2(a) shows the ion velocity obtained over several shots, taken at various laser and target parameters, plotted against a parameter 'Ω = target thickness/HB velocity'. The HB velocity is calculated from the expression, $c\ \bar{\Xi}/(1+\ \bar{\Xi})$, where $\Xi = I/\rho c^3$ and c is the speed of light in vacuum [6]. 'Ω'

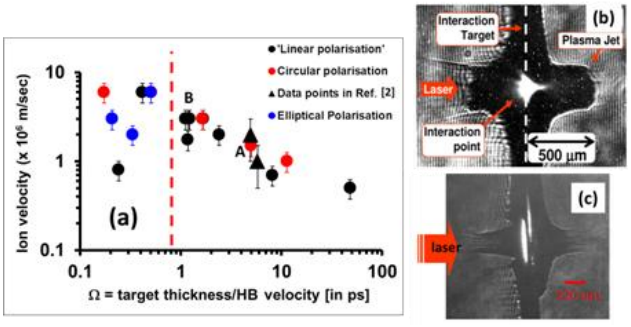

Fig 2. (a) Graph showing estimated ion velocity for different value of Ω, a parameter that depends on the laser and target parameters (as explained in the text). The red dotted line indicates the pulse duration of laser used in our experiment. (b) and (c) shows the interferograms correspond, respectively, to the data points 'A' and 'B' in (a).

corresponds to the time required by the HB ions from the target front surface to reach the rear. As expected, because of collisional energy loss by the ions in the bulk of the target, the ion velocity falls gradually as Ω increases. The ion velocity attains maximum value when the incidence laser pulse duration is comparable to Ω. Lowering further the parameter Ω, by increasing the laser intensity, or, by decreasing the target density or thickness, the plas ma jet start to lose their cohesion, forming filamentary features (see Fig. 2(c)). The loss of uniformity appears to be faster for linear polarisation of incident laser compared to circular polarisation, most likely due to significantly higher fast electron heating of the target for linear polarised laser interaction [4,5]. Detail analysis of the data is currently under progress. However, it is anticipated that the loss of cohesion of jets for Ω ~ incident laser pulse duration, is as a result of complete hole boring of target before the end of the incidence laser pulse. In fact, for significantly lower value of Ω, we could not able to observe a sustained jet formation, even for 100s of ps duration.

(b) LS-TNSA hybrid acceleration

In case of Ω ≤ 1, i.e. for very thin targets, ion spectra along target normal direction showed peaked feature towards higher energy side of the spectrum as shown in the Fig. 3(a). This is by contrast to the quasi-maxwellian spectra obtained for Ω>1 (see Fig. 3(b) for instance).

Since for the ultra-thin targets, HB accelerated ions from the target front surface reach the target rear surface within a fraction of laser pulse duration (0.1 ps for the case shown in the Fig. 3(a)), the remaining duration of the CPA is spent in accelerating the ions in LS regime which has resulted in a peaked spectral feature in both the heavy ion and proton spectra. Ion energy attained by the LS mechanism scales with the ratio between laser intensity and target areal density, given by [4,5] $\beta_{LS} = \frac{(1+\psi)^2-1}{(1+\psi)^2+1}$, where $\psi = 2\pi \frac{Z}{A}\frac{m_e}{m_p}\frac{a_o^2 \tau_{LS}}{\zeta}$. Here $a_o = 0.85\ \overline{I\lambda^2/10^{18}\, Wcm^{-2}\mu m^2}$ is dimensionless laser amplitude; λ is the laser wavelength, n_e and l are the electron density and thickness of the compressed layer. τ_{LS} is the duration of the laser pulse used for LS acceleration. Z and A are the atomic number and mass number of the target ions, and, m_e and m_p are the masses of an electron and proton respectively. Using the laser and target parameters for the case shown in the Fig. 3(a) in a

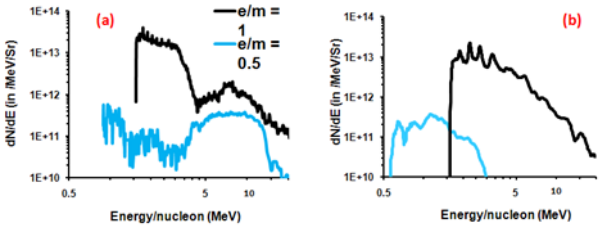

Fig 3. Experimental obtained spectra of two ion species for (a) thin (100 nm) and (b) thick (10 um) Cu targets irradiated at similar laser intensity and polarisation, which correspond to Ω ~ 0.1 and 10 respectively.

simple numerical modeling based on the LS equation, we found that ion energy of 8 MeV/nucleon is expected by the LS mechanism, which agrees well with the experimental data (see the data point 'A' in the Fig. 4). Particle-in-cell simulation carried out for a scaled down laser and target parameters also shows quasi-monoenergetic peak in ion spectra around 10 MeV/nucleon, which further substantiate the role of LS mechanism during the interaction.

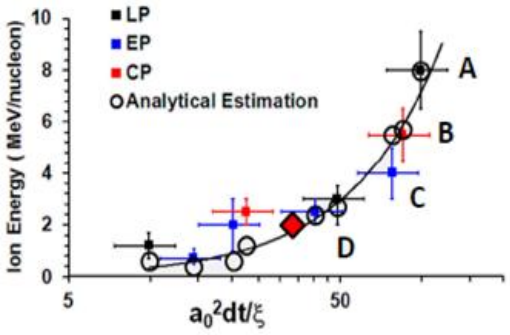

Fig 4: Graph showing the peak energy (/nucleon) of the ions (e/m=0.5) obtained experimentally for different laser and target parameters, plotted against the parameter . The red diamond with the black outer line represents the previously reported experimental data by Heing et. al.[3]. The experimental parameter set (intensity, target material, target thickness) for the data points marked as A, B, C and D are (3×10^{20} W/cm^2, Cu, 0.1μm), (1.25×10^{20} W/cm^2, Cu, 0.05μm), (2.2×10^{20} W/cm^2, Cu, 0.1μm), (6×10^{19} W/cm^2, Al, 0.1μm) respectively. The circles represent the results from simple numerical modeling based on the eq. (1). Data point 'A' corresponds to the case shown in the Fig. 3(a).

The scaling of RPA-LS mechanism has been obtained by a methodical scan over a range of target thickness, density, laser intensity and polarization. Fig 4 shows Ion energy scaling with the relevant scaling parameter $a_o^2\tau_{LS}/\zeta$. The data provide compelling experimental evidence for dominance of LS acceleration over TNSA. We can also see that, there is a good agreement between experimental data and RPA estimation for the other data points in the rising slope of the trend in the Fig. 4. The experimental data points shows that the ion energy scales with $(a_o^2\tau_{LS}/\zeta)^{1.5}$, which is significantly faster than the TNSA scaling, $E \propto a_o$.

Conclusion:

The role of the radiation pressure of an intense laser beam in the formation of narrow band proton and carbon spectra has been discussed. The data presented show that the onset of the LS regime of RPA can be obtained at currently available laser intensity, in competition with the TNSA mechanism.

References:

[1] M. Borghesi *et. al.*, Fusion Science and Technology, 49, 412 (2006) and the references therein.

[2] S. Kar *et al*, Phys. Rev. Lett., 100, 225004 (2008).

[3] A. Heing *et. al.,* PRL 103, 245003 (2009).

[4] A. Robinson et. al., New. J. Phys. 10, 013021 (2008); B. Qiao et. al., Phys. Rev. Lett. 102, 145002 (2009).

[5] A. Macchi et., al., Phys. Rev. Lett. 94, 165003 (2005); A. Macchi et. al, New J Phys., 12, 045013 (2010).

[6] A P L Robinson, et. al., Plasma Phys. Control. Fusion 51, 024004 (2009).